Epigenome editing reveals core DNA methylation for imprinting control in the *Dlk1-Dio3* imprinted domain

Shin Kojima[1],[†], Naoya Shiochi[1],[†], Kazuki Sato[1], Mamiko Yamaura[1], Toshiaki Ito[1], Nodoka Yamamura[1], Naoki Goto[1], Mika Odamoto[1], Shin Kobayashi[2], Tohru Kimura[1],[*] and Yoichi Sekita [1],[*]

[1]Laboratory of Stem Cell Biology, Department of Biosciences, Kitasato University School of Science, 1-15-1 Kitasato, Minami-ku, Sagamihara, Kanagawa 252-0373, Japan and [2]Cellular and Molecular Biotechnology Research Institute, National Institute of Advanced Industrial Science and Technology, 2-4-7 Aomi, Koutou-ku, Tokyo 135-0064, Japan

ABSTRACT

The *Dlk1-Dio3* imprinted domain is controlled by an imprinting control region (ICR) called IG-DMR that is hypomethylated on the maternal allele and hypermethylated on the paternal allele. Although several genetic mutation experiments have shown that IG-DMR is essential for imprinting control of the domain, how DNA methylation itself functions has not been elucidated. Here, we performed both gain and loss of DNA methylation experiments targeting IG-DMR by transiently introducing CRISPR/Cas9 based-targeted DNA methylation editing tools along with one guide RNA into mouse ES cells. Altered DNA methylation, particularly at IG-DMR-Rep, which is a tandem repeat containing ZFP57 methylated DNA-binding protein binding motifs, affected the imprinting state of the whole domain, including DNA methylation, imprinted gene expression, and histone modifications. Moreover, the altered imprinting states were persistent through neuronal differentiation. Our results suggest that the DNA methylation state at IG-DMR-Rep, but not other sites in IG-DMR, is a master element to determine whether the allele behaves as the intrinsic maternal or paternal allele. Meanwhile, this study provides a robust strategy and methodology to study core DNA methylation in *cis*-regulatory elements, such as ICRs and enhancers.

INTRODUCTION

Genomic imprinting is a phenomenon unique to placental mammals among vertebrates, in which maternal and paternal genomes are functionally different. This difference arises from parent-of-origin-specific allelic expression of imprinted genes (1). In most cases, multiple imprinted genes form a cluster on a chromosome, and monoallelic expression of each gene throughout a cluster is regulated by a *cis*-regulatory element called the imprinting control region (ICR). ICRs exhibit differential DNA methylation and histone modifications between alleles, and such differential epigenetic modifications are thought to be critical for monoallelic expression of imprinted genes. Differential DNA methylation at ICRs is established during gametogenesis, and some, but not all, ICRs contain tandem repeat arrays that are important regulators of DNA methylation (2–4). A critical feature of ICRs is that although the most of DNA methylation is erased across the genome after fertilisation in a process called epigenetic reprogramming, that of ICRs persists through this process. Krüppel-associated box (KRAB)-containing zinc finger protein (KRAB-ZFP)-TRIM28 (also known as KAP1 or TIF1β) complex, which contains a methylated DNA-binding protein such as ZFP57, ZFP445 or ZNF202, binds to methylated ICRs to maintain DNA methylation during epigenetic reprogramming after fertilisation (5–7). Therefore, circumstantial evidence suggests that DNA methylation at ICRs is important for maintenance of the imprinting state.

The *Dlk1-Dio3* imprinted domain contains three paternally expressed protein-coding genes, *Dlk1*, *Rtl1* (also known as *Peg11*) and *Dio3*, along with several maternally expressed non-coding transcripts, such as *Meg3*, *Rtl1as*, *Meg8* (also known as *Rian*) and *Mirg*, and has an important role in the normal development of both humans and mice (8–13). The intergenic differentially methylated region (IG-DMR), which resides in the intergenic region between *Dlk1* and *Meg3*, is hypermethylated on the paternal allele

(methylated during spermatogenesis), and hypomethylated on the maternal allele, in somatic cells, preimplantation embryonic cells, and embryonic stem cells (ESCs) (14). Knockout mice lacking the entire IG-DMR demonstrated its critical role in imprinting regulation of the whole *Dlk1-Dio3* domain; in other words, IG-DMR functions as the ICR of the domain (15). Several recent studies have shown that IG-DMR is a bipartite element that consists of 5′ IG^{CGI} (CGI: CpG island) and 3′ IG^{TRE} (TRE: transcriptional regulatory element) (4,16,17). IG^{CGI} contains a 216-bp tandem repeat called IG-DMR-Rep, and its deletion in mice revealed an essential role of IG-DMR-Rep in the maintenance of DNA hypermethylation on the paternal allele after fertilisation (4,18). On the other hand, unmethylated IG^{TRE} of the maternal allele functions as an enhancer of *Meg3* (16,19–21). *Meg3*-DMR, which is located in the *Meg3* promoter, acquires DNA methylation on the paternal allele at the postimplantation stage, whereas the maternal allele remains hypomethylated (22). In addition to *in vivo* and *ex vivo* genetic experiments, human cases associated with Kagami-Ogata and Temple syndromes (KOS and TS, respectively) show DNA methylation abnormalities (i.e. epimutations) at IG-DMR (9,23,24). These observations strongly suggest that DNA methylation at IG-DMR is the pivotal element for imprinting regulation of the domain. However, there is a lack of experimental evidence of a causative role of abnormal DNA methylation at IG-DMR rather than other epigenetic modifications in altered imprinted gene expression or phenotypes associated with the domain. Additionally, it is not clear whether IG-DMR-Rep functions in the maintenance of hypomethylation on the maternal allele. This is because of a lack of experimental strategies for manipulating DNA methylation in a site-specific manner.

Recently, several epigenome editing tools based on genome editing technologies have been developed (25). These tools make it possible to edit epigenetic modifications in a site-specific manner by utilizing epigenetic modifier proteins fused with the guide RNA (gRNA)-dependent targeted DNA-binding protein of the bacterial clustered regularly interspaced short palindromic repeat (CRISPR)/Cas9 system. Although several epigenome-editing tools have been proposed, there is still no gold standard. Particularly, direct fusion of catalytically inactive Cas9 (dCas9) and epigenetic modifiers may show limited effects on epigenome editing, probably because they function in a context-dependent manner, such as targeted genomic regions or cell types (26–28). Among such tools, systems combining the CRISPR/Cas9 system and the SunTag-scFv system, together with DNA demethylation factor TET1 or DNA methyltransferase 3A (DNMT3A), can efficiently demethylate or methylate target genomic DNA, respectively (27,28). In these systems, dCas9 fused with GCN4 peptide is recruited to gRNA-dependent target genomic sites, and the GCN4 peptide-recognising single-chain variable fragment (scFvGCN4) antibody fused with the TET1 or the DNMT3A catalytic domain (TET1CD or DNMT3A) is also recruited to the target sites. When TET1CD is used, it oxidizes methylcytosine into hydroxymethylcytosine at target sites to trigger the DNA demethylation process (27). By contrast, when DNMT3A is used, it methylates the target DNA (28).

In this study, to focus on the role of DNA methylation per se rather than DNA sequence or other epigenetic modifications at IG- and *Meg3*-DMRs, we applied these systems to induce hypo- or hypermethylation at the targeted DMRs in mouse ESCs by transient expression of DNA methylation editing proteins. Both loss and gain of DNA methylation at IG-DMR-Rep, but not other sites in IG- or *Meg3*-DMRs, affected the whole of the *Dlk1-Dio3* imprinted domain in terms of imprinted gene expression and histone modifications, even after induction of neuronal differentiation. These results provide direct evidence for DNA methylation at IG-DMR-Rep as a pivotal element in regulation of the domain.

MATERIALS AND METHODS

ESC establishment and culture conditions

The BJ ESC line was established from a male blastocyst of F1 hybrid between female C57BL/6 and male JF1 mice without using two inhibitors (CHIR99021 for GSK-3 and PD0325901 for MEK) because they affect DNA methylation level in ESCs (29,30). The F1 hybrid blastocysts were produced by an *in vitro* fertilisation (IVF) method. After about 4 days of culture using KSOM medium, expanded blastocysts were plated into gelatin-coated dishes with monolayers of mouse embryonic fibroblasts (MEFs). The medium used was ES cell derivation medium consisting of KnockOut DMEM (Thermo Fisher) supplemented with 20% fetal calf serum (BioWest), 0.1 mM nonessential amino acids, 1 mM sodium pyruvate, 0.1 mM 2-mercaptoethanol, 0.5 mg/ml penicillin–streptomycin–glutamine solution (all from Invitrogen), and 3000 U/ml mouse leukemia inhibitory factor (LIF) (Millipore). Four to seven days after plating, inner cell mass outgrowths were transferred into 20 μl 0.25% trypsin–EDTA (Invitrogen), dissociated by pipetting and plated on MEFs. Undifferentiated ES cell colonies were expanded to establish ES cell lines, and used for further analysis. The established BJ ESCs were maintained on gelatinised tissue culture dishes without feeder MEFs under serum/LIF conditions, i.e. DMEM-high glucose (Nacalai Tesque) supplemented with 10% FCS (Japan Bio Serum), 100 U/ml LIF (made in-house), 0.1 mM 2-mercaptoethanol (Sigma-Aldrich), penicillin/streptomycin (Nacalai Tesque), 2 mM L-glutamine (Nacalai Tesque) and 1× nonessential amino acids (Nacalai Tesque).

Neuronal differentiation

BJ ESCs transfected with DNA methylation editing components at D7 or later were cultured in SFEB condition followed by adhesive condition based on the method described previously with some modifications (31). Briefly, 1.6×10^6 BJ ESCs were cultured floatingly for 7 days on non-treated 60-mm dishes in the neuron differentiation medium; G-MEM L-glutamine (Nacalai Tesque), supplemented with 10% KnockOut Serum Replacement (Thermo Fisher), 2 mM glutamine (Nacalai Tesque), 1 mM sodium pyruvate (Nacalai Tesque), 0.1 mM 2-mercaptoethanol (Sigma-Aldrich) and 1× nonessential amino acids (Nacalai Tesque). Then, the formed spheroids were transferred onto

poly-D-lysin- and laminin-coated six-well plates for adhesive culture for 7 days in the N2 medium; G-MEM L-glutamine (Nacalai Tesque), supplemented with 1× N-2 Supplement (Thermo Fisher), 2 mM glutamine (Nacalai Tesque), 1 mM sodium pyruvate (Nacalai Tesque), 0.1 mM 2-mercaptoethanol (Sigma-Aldrich) and 1× nonessential amino acids (Nacalai Tesque). Totally 14 days after starting the floating culture, cells were scraped, collected into tubes, snap-frozen in liquid nitrogen and stored at –80°C until DNA and RNA extractions. Three independent differentiation experiments with duplicate for each (i.e. total $n = 6$) were performed, and the average of the gene expression and DNA methylation of the cells transfected with the scr gRNA of each experiment were set to 1. The relative levels of the cells transfected with gR2 and NTF cells were calculated.

Mice

C57BL/6 mice were purchased from Japan SLC. JF1 mice were bred in the laboratory. All animal care and experiments were carried out in accordance with the Guidelines for Animal Experiments of Kitasato University, and were approved by Institutional Animal Care and Use Committee of Kitasato University (SAS2104-Animal Experiment Committee, Kitasato University School of Science).

Plasmid construction

For a backbone to construct pX330-dCas9GCN4-P2A-Puro, pX330 (Addgene plasmid #42230) was double digested with EcoRI and AgeI to excise Cas9. dCas9-GCN4 without the stop codon was amplified from Addgene plasmid #82560 by PCR. The three DNA fragments, i.e. the backbone, dCas9-GCN4, and P2A-Puro^R, amplified by PCR (with a synonymous mutation at the BbsI site) were fused by In-Fusion Cloning Enzyme according to the manufacturer's protocol (Takara). See Supplementary Table S2 for PCR primer sequences.

To clone guide RNA, pX330-dCas9GCN4-P2A-Puro was digested with BbsI, and then double-stranded oligo DNA was ligated as described previously (32). See Supplementary Table S3 for gRNA sequences.

Transfection

For reverse-transfection, $1.6 × 10^6$ BJ ESCs were plated in each gelatinised well of a 6-well plate on the day of transfection (D0), and then transfected with 0.7 µg of pX330-dCas9GCN4-P2A-Puro and 1.1 µg of pCAG-scFvGCN4sfGFPTET1CD for the loss of DNA methylation experiment or 0.7 µg of pEF1a-NLS-scFvGCN4-DNMT3A for the gain of DNA methylation experiment using Lipofectamine 3000 (Thermo Fisher), in accordance with the manufacturer's instructions. From 24 h posttransfection, transfected cells were selected with 1.0 µg/ml puromycin-containing medium for 30 h (D1–D2), and complete selection for each experiment was confirmed by observing the disappearance of nontransfected cells that were seeded and cultured under the same conditions as the transfected cells. Each combination of plasmids was transfected into three wells, and cultured and sampled independently for experimental triplicates. Cells were sampled on D3 and D7 by trypsinisation and the cell pellets were snap-frozen in liquid nitrogen. The pellets were stored at –80°C until DNA and RNA extraction.

Bisulfite-PCR/amplicon-seq

DNA was extracted by lysing cell pellets with ProK/Lysis buffer (2 mg/ml proteinase K, 50 mM Tris–HCl, pH 8.0, 0.1 M NaCl, 20 mM EDTA, 1% SDS) at 55°C overnight. The lysate was applied to the bisulfite reaction and subsequent PCR, sequencing by Illumina-Miseq, and quantification of methylation as described previously (33). The primers used for bisulfite PCR are listed in Supplementary Table S2. The number of sequenced reads and methylation level of each sample are shown in Supplementary Data S1.

Quantitative RT-PCR (RT-qPCR) and RT-PCR/amplicon-seq

Total RNA was isolated from cells using an RNeasy Mini Kit (QIAGEN) according to the manufacturer's instructions. Reverse transcription (RT) was performed using the ThermoScript RT-PCR System (Invitrogen) and an oligo (dT) + adaptor primer under conditions of 50°C for 50 min and 85°C for 5 min (22).

RT-qPCR was performed using a real time PCR system (CFX384; Bio-Rad), and expression levels of genes except for *Rtl1* were measured using THUNDERBIRD Next SYBR qPCR Mix (Toyobo) by PCR with an initial denaturation step at 95°C for 30 s followed by 40 cycles of 95°C for 5 s and 60°C for 30 s. As *Rtl1* is transcribed from the same genomic region as *Rtl1as* in the opposite direction (34), to amplify *Rtl1* specifically, we performed RT-qPCR by adapting 3′-RACE as described previously with some modifications (22). Briefly, 3′-RACE RT-qPCR was performed in a 10 µl PCR mixture including 1 × buffer for KOD -Multi & Epi- (Toyobo), 0.83 × SYBR Green I (Takara), 0.5 µM each of primer (adaptor, and *Rtl1*-specific primer), and 20 mU KOD -Multi & Epi- polymerase (Toyobo) by PCR with an initial denaturation step at 94°C for 2 min followed by 40 PCR cycles of 98°C for 10 s, 70°C for 5 s, and 74°C for 30 s (CFX384; Bio-Rad). We performed absolute quantification by drawing standard curves using genomic DNA as templates for the genes except *Rtl1*, and a plasmid cloned from the PCR amplicon of 3′-RACE for *Rtl1*. *Arbp* (ribosomal protein, large, P0) was used as an internal control. The RT and PCR primers are listed in Supplementary Table S2.

For RT-PCR/amplicon-seq, conventional RT-PCR was first performed using KOD -Multi & Epi- (Toyobo) using specific primers containing an Illumina sequence adaptor with an initial denaturation step at 94°C for 2 min followed by 33–35 cycles of 98°C for 10 s, 55 or 58°C for 30 s and 68°C for 30 s. See Supplementary Table S2 for primer sequences and annealing temperatures. The first PCR products were cleaned up with NucleoMag NGS Clean-up and Size Select (Takara), and the adaptor for sequencing was applied to the resulting PCR products using a Nextra XT index kit

(Illumina) by five cycles of second PCR. The second PCR products were cleaned up with NucleoMag NGS Clean-up and Size Select (Takara) and sequenced with an Illumina Miseq system using Miseq Reagent Nano Kit v2 (500 Cycles) (Illumina). Sequence reads were analyzed for allelic expression by counting the number of reads containing SNPs of C57BL/6 or JF1. The number of sequenced reads and allelic ratio of each sample are shown in Supplementary Data S2.

ChIP-qPCR and ChIP-PCR/amplicon-seq

Chromatin immunoprecipitation (ChIP) was performed based on the procedure described previously with modifications (35). Briefly, 1×10^6 trypsinised ESCs on D7 were sampled and suspended in culture medium, fixed with 1% paraformaldehyde (PFA) for 10 min at room temperature, exposed to 125 mM glycine to terminate crosslinking, and then washed twice with ice-cold PBS. To isolate nuclei, the cells were incubated for 10 min on ice in cell lysis buffer (CLB; 10 mM Tris–HCl, pH 8.0, 1 mM EDTA, 0.5% NP-40, 1× protease inhibitor cocktail), and then chromatin was isolated by incubating nuclei in nuclear lysis buffer (NLB; 10 mM Tris-HCl, pH 8.0, 1 mM EDTA, 0.5 M NaCl, 1% Triton X-100, 0.5% sodium deoxycholate, 0.5% lauroylsarcosine, 1× protease inhibitor cocktail) on ice for 10 min followed by washing with ice-cold PBS. The chromatin was resuspended in 150 µl modified lysis buffer 3 (MLB3; 10 mM Tris-HCl, pH 8.0, 1 mM EDTA, 0.5 mM EGTA, 150 mM NaCl, 0.1% sodium deoxycholate, 0.1% SDS, 1× protease inhibitor cocktail), and then fragmented by sonication using a Bioruptor (energy High, 25 cycles of ON for 30 s and OFF for 30 s by keeping the water of the sonicator bath cold). Subsequently, 1.2 ml ChIP dilution buffer (16.7 mM Tris-HCl, pH 8.0, 167 mM NaCl, 1.2 mM EDTA, 0.01% SDS, 1% Triton X-100) was added to the fragmented chromatin, and the supernatant after centrifugation was collected for incubation with antibodies. The chromatin–antibody complex was precipitated using Protein G Sepharose 4 Fast Flow (Merck) and the chromatin was washed in a step-by-step manner using wash buffers in accordance with the standard ChIP procedure. After decrosslinking and RNase and proteinase K treatment, DNA was purified using a Cica Geneus PCR & Gel Prep Kit (Kanto Chemical) according to the manufacturer's protocol.

For qPCR, we used THUNDERBIRD Next SYBR qPCR Mix (Toyobo) with an initial denaturation step at 95°C for 30 s followed by 40 cycles of 95°C for 5 s and 60°C 30 s. For ChIP-PCR/amplicon-seq, see the Quantitative RT-PCR (RT-qPCR) and RT-PCR/amplicon-seq section. The primer sequences used in the assay are listed in Supplementary Table S2. Antibodies are as follows, Rabbit polyclonal anti-Histone H3 (Abcam, Cat# ab1791), Rabbit IgG (Upstate, Cat# PP64B), Rabbit polyclonal anti-H3K4me3 (Active Motif, Cat# 39915), Rabbit polyclonal anti-H3K27ac (Active Motif, Cat# 39133), Rabbit polyclonal anti-H3K9me3 (Abcam, Cat# ab8898), and Rabbit polyclonal anti-ZFP57 (Abcam, Cat# ab45341). The number of sequenced reads and allelic ratio of each sample are shown in Supplementary Data S3.

Statistical analysis

To evaluate the effects of DNA-methylation editing on DNA methylation, gene expression and chromatin state in undifferentiated ESCs, each combination of plasmids was transfected into cells in three wells of six-well plates, which were cultured and sampled independently for experimental triplicates. For neuronal differentiation experiments, each combination of plasmids was transfected into cells in two wells of six-well plates, which were cultured and differentiated into neural precursors in three independent experiments to confirm reproducibility of differentiation. Statistical analyses of DNA methylation, RT-qPCR and ChIP-qPCR results were performed using the unpaired Student's *t* test. Data are shown as means with error bars representing the standard deviation.

RESULTS

Experimental scheme and design of guide RNAs for targeted DNA methylation editing at IG- and *Meg3*-DMRs

We used mouse ESCs established from F1 hybrids between female C57BL/6 (B6) (*Mus musculus musculus*) and males of its subspecies JF1 (*Mus musculus molossinus*), called BJ ESCs. The BJ ESCs enabled us to quantify allelic DNA methylation, gene expression, and histone modifications based on single-nucleotide polymorphisms (SNPs) between B6 (maternal) and JF1 (paternal) alleles. For site-specific DNA methylation editing, we used pCAG-scFvGCN4sfGFPTET1CD (Addgene plasmid #82561) (27) for DNA demethylation (loss of DNA methylation experiment) or pEF1a-NLS-scFvGCN4-DNMT3A (Addgene plasmid #100941) (28) for DNA methylation (gain of DNA methylation experiment) (Figure 1A). To express the dCas9-GCN4 fusion protein and a single gRNA from the same plasmid, we constructed pX330-dCas9GCN4-P2A-Puro, a plasmid carrying dCas9-GCN4 fusion protein (adapted from Addgene plasmid #82560) and a gRNA under the control of the U6 promoter, as well as a Puro^R cassette connected to the 3′ end of dCas9-GCN4 through the P2A peptide. We transiently transfected BJ ESCs with the two plasmids by lipofection and selected transfected cells with puromycin for 30 h from day 1 post-transfection (D1) (Figure 1B). Cells were sampled on D3 or D7 for further analysis (Figure 1B). Each gRNA-expressing plasmid was transduced into cells on three wells of six-well plates, and each was cultured and sampled independently.

We designed six gRNAs (gR1–5 and gR7) corresponding to sequences within the IG-DMR and a gRNA corresponding to a sequence within *Meg3*-DMR (gR6) (Figure 1C). IG-DMR can be divided into two subdomains, i.e. IG^CGI and IG^TRE comprising the 5′- and 3′-halves of IG-DMR, respectively (16) (Figure 1D). Two gRNAs (gR1 and gR2) corresponded to sequences in IG^CGI in which histone H3-K4 trimethylation (H3K4me3) is enriched. Notably, gR2 corresponded to a sequence within IG-DMR-Rep. Another three gRNAs (gR4, gR5 and gR7) were designed within
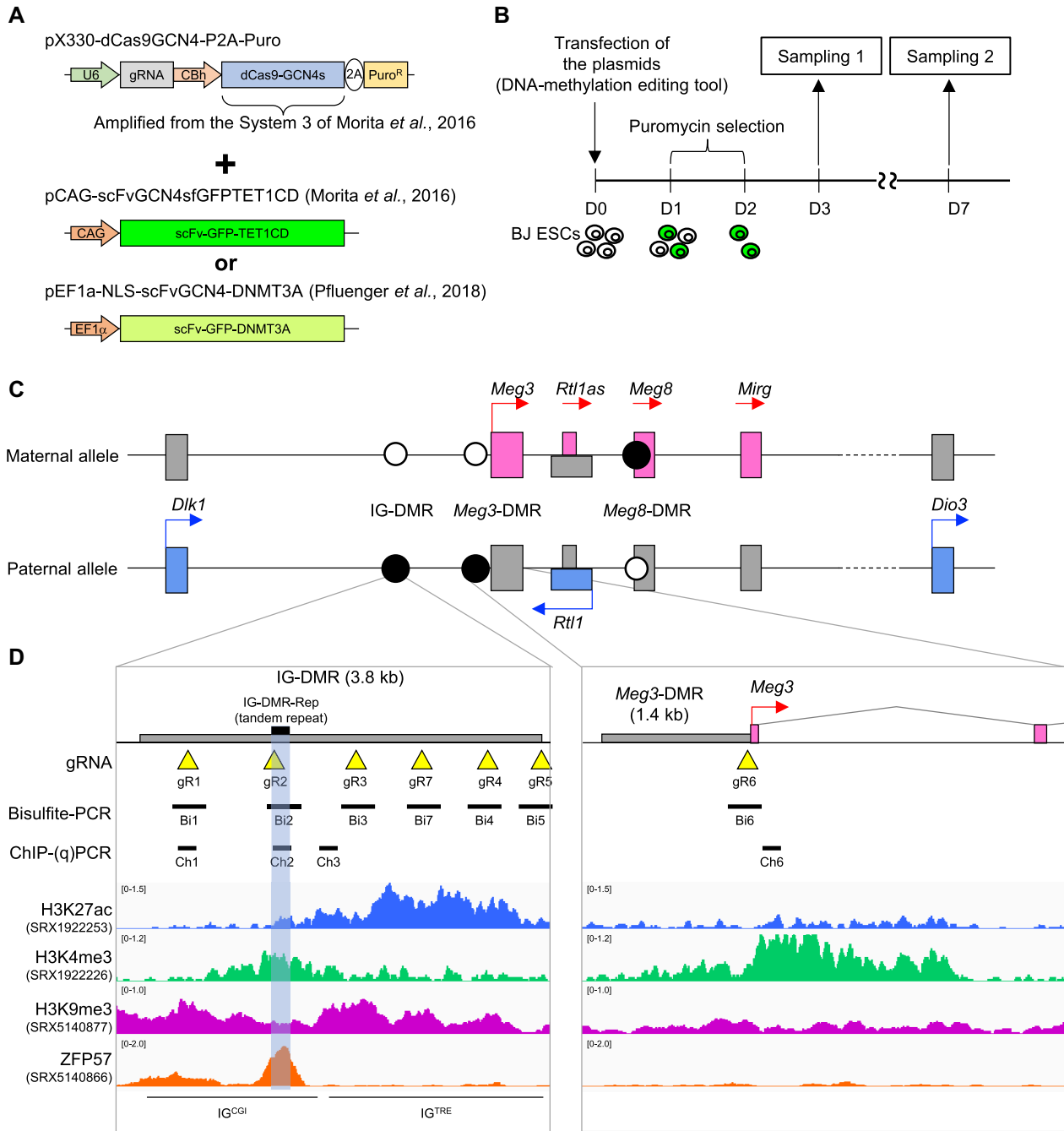
Figure 1. Experimental scheme and design of guide RNAs for targeted DNA-methylation editing at IG- and *Meg3*-DMRs. (**A**) DNA methylation editing tools used in targeted loss and gain of DNA methylation experiments. (**B**) Experimental scheme. (**C**) Genomic structure of mouse *Dlk1-Dio3* imprinted domain in normal cells. Red and blue boxes represent maternally and paternally expressed genes, respectively. Gray boxes represent repressed genes. Filled and open circles represent hyper- and hypomethylated differentially methylated regions (DMRs), respectively. (**D**) Guide RNA (gRNA) targeting sites (yellow triangles) and bisulfite- and ChIP-(q)PCR sites (black bars) at IG- and *Meg3*-DMRs. IG-DMR-Rep is shaded in light blue. Chromatin features (H3K4me3, H3K27ac and H3K9me3) and ZFP57 binding state in ESCs were adapted from the ChIP-Atlas (57).

IG^{TRE} in which H3-K27 acetylation (H3K27ac), the active enhancer mark, is enriched. gR3 was designed corresponding to the border of the subdomains.

Targeted DNA demethylation at IG-DMR-Rep by one gRNA leads to persistent and outspread DNA hypomethylation to IG- and *Meg3*-DMRs

Before performing targeted DNA demethylation, we investigated the DNA methylation states at IG- and *Meg3*-DMRs of the BJ ESCs without transfection (non-transfected cells, NTF cells) and cells transfected with scrambled (scr) gRNA that does not have any targets in the mouse genome, dCas9GCN4-P2A-Puro, and scFvGCN4sfGFPTET1CD (the demethylation tool). We quantified DNA methylation by bisulfite-PCR followed by amplicon sequencing by Miseq instead of conventional TA-cloning followed by Sanger sequencing. Six bisulfite-PCR primer sets were designed to amplify 260–480 bp DNA each of which included one of the targets of the gRNAs (Bi1–Bi6) (Figure 1D). Sequenced bisulfite-PCR amplicons were computationally divided into maternal or paternal alleles depending on SNPs except for the Bi4 amplicon that did not contain any informative SNPs. Analysis of NTF cells revealed all bisulfite PCR sites except Bi4 were hypomethylated on the maternal allele and hypermethylated on the paternal allele, and about 50% methylated at the Bi4 site, indicating that the DNA methylation states at IG- and *Meg3*-DMRs of the BJ ESCs used in this study were the same as in normal somatic cells *in vivo* (14,36) (Figure 2A and Supplementary Figure S1A). Moreover, DNA methylation in cells transfected with scr gRNA on D3 and D7 showed no significant differences compared to NTF cells, indicating that the DNA demethylation tool used here does not have nonspecific (i.e. gRNA-independent) DNA demethylation activity (Figure 2A and Supplementary Figure S1A).

Next, we investigated DNA methylation of cells transfected with one of the gRNAs (gR1–gR6). On D3, DNA methylation at each target site, e.g. Bi1 site in cells transfected with gR1, was significantly reduced to 45–80% compared to cells transfected with scr gRNA (Figure 2B, upper panel and Supplementary Figure S1B), indicating that the gRNAs designed here functionally recruited the DNA demethylation components. On D7, cells with gR2 targeting IG-DMR-Rep showed 40–60% hypomethylation at all sites in IG- and *Meg3*-DMRs compared to cells transfected with scr gRNA (Figure 2B, lower panel and Supplementary Figure S1C). The methylation level of cells transfected with gR1 and gR3 remained lower, whereas cells transfected with gR4 or gR5 targeting IG^{TRE} relapsed to similar levels to cells transfected with scr gRNA. Cells transfected with gR6 remained hypomethylated at *Meg3*-DMR on D7, but it did not affect IG-DMR methylation. On the other hand, DNA methylation was unaffected when transfected with the DNA demethylation tool in which TET1 is catalytically inactive along with gR2, indicating that the DNA methylation changes observed here were dependent on the hydroxymethylation activity of the exogenous TET1CD. Moreover, it was suggested that the hypomethylation induced by gR2 was not due to steric hindrance brought about by the DNA demethylation components against endogenous proteins that intrinsically bind to the gR2-targeting site (Figure 2B and Supplementary Figure S1D).

IG-DMR-Rep contains a tandem repeated array sequence with five ZFP57 binding motifs. ZFP57 binds to the motif when its DNA is methylated. Consistent with the decreased DNA methylation level, ChIP-qPCR using the Ch2 primer set on D7 showed significant reduction of ZFP57 binding to IG-DMR-Rep in cells transfected with gR2 compared to those transfected with scr gRNA (Figure 2C). *Pank4* and *Gapdh* genomic loci were used as positive and negative controls, respectively (37) (Figure 2C). These results indicate that induced DNA hypomethylation at IG-DMR-Rep is persistent for at least 7 days, and outspreads to the entire IG-DMR and *Meg3*-DMR, which is 8.5 kb away from IG-DMR, as well as inhibiting ZFP57 binding.

Loss of DNA methylation at IG-DMR-Rep disrupts monoallelic maternal expression of *Meg3* and *Mirg*, and allele-specific histone modifications

We investigated expression levels and alleles of *Meg3* and *Mirg* on D7. We performed two types of RT-PCR using each cDNA, both of which amplified the same or overlapping regions, including SNPs between B6 and JF1 (Figure 2D). One was conventional RT-qPCR, and the other was normal RT-PCR followed by amplicon sequencing using Miseq to distinguish expression alleles (hereafter, this method is referred to as 'RT-PCR/amplicon-seq'). Then, we calculated the expression levels from each allele by combining RT-qPCR results and the ratios of the read numbers of B6 (maternal) and JF1 (paternal) alleles (Figure 2D). We used genomic DNA of the BJ ESCs as a control to analyse the allelic ratio, and found an approximately 1:1 read number ratio between B6 and JF1 alleles, indicating limited artificial bias of this analysis (Supplementary Data 2, related to Figure 2D).

The cells transfected with gR1 and gR2 showed 1.5-fold ($P = 0.027$, $n = 3$) and 2.1-fold ($P = 0.027$, $n = 3$) upregulation of *Meg3*, and 1.5-fold ($P = 0.0014$, $n = 3$) and 2.2-fold ($P = 3.1 \times 10^{-5}$, $n = 3$) upregulation of *Mirg* relative to controls transfected with scr gRNA, respectively (Figure 2E). No significant differences in expression were observed in cells transfected with other gRNAs. The combination of RT-qPCR and RT-PCR/amplicon-seq revealed that the upregulation was due to expression from the paternal allele. Interestingly, the stronger effect on DNA demethylation by gR2 than by gR1 (paternal allele methylation levels of 40% and 60%, respectively) caused higher elevation of *Meg3* and *Mirg* expression from the paternal allele. Notably, although *Meg3*-DMR was persistently hypomethylated by gR6 on D7, neither *Meg3* nor *Mirg* expression was altered (Figure 2B and E).

Next, we investigated the effects of induced DNA hypomethylation at IG-DMR-Rep on histone modifications. In normal ESCs, H3K4me3 and H3K27ac were enriched on IG^{CGI} and IG^{TRE}, respectively (Figure 1D). We performed a combination of quantitative ChIP-PCR (ChIP-qPCR) and normal ChIP-PCR followed by amplicon-sequencing by Miseq (hereafter referred to as 'ChIP-PCR/amplicon-seq') on D7 (Figure 2F). This analysis showed that the levels of H3K4me3 and H3K27ac at IG-DMR (PCR primer set;
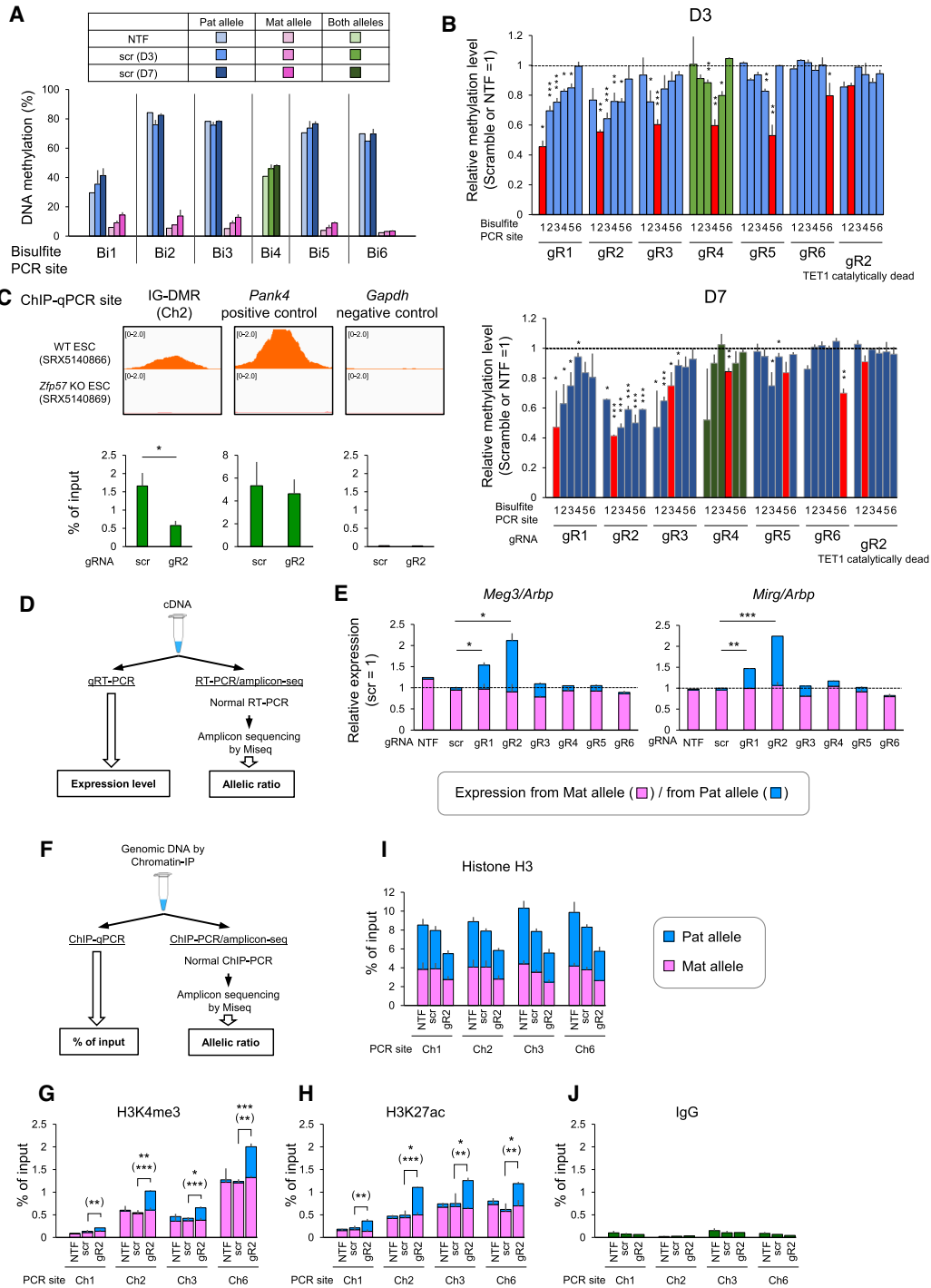
Figure 2. Effects of targeted loss of DNA methylation at IG- and *Meg3*-DMRs. (**A**) DNA methylation levels at IG-DMR (Bi1–5) and *Meg3*-DMR (Bi6) in nontransfected (NTF) and scramble (scr) gRNA-transfected BJ ESCs on D3 and D7. Paternal and maternal alleles were separated except for Bi4, which is shown for both alleles. (**B**) DNA methylation levels relative to scr gRNA-transfected cells for gR1–gR6 and to NTF cells for gR2 with catalytically inactive TET1 at D3 and D7 (upper and lower panels, respectively). DNA methylation levels of the paternal allele are shown except for the Bi4 site, which is shown for both alleles. Red bars indicate bisulfite-PCR sites corresponding to gRNA target sites. (**C**) ChIP-qPCR for ZFP57 at the Ch2 site in IG-DMR. Genomic loci of *Pank4* and *Gapdh* that were not targeted by gR2 were used as the positive and negative controls, respectively (37). ZFP57 binding states at each locus in WT and *Zfp57*-KO ESCs were adapted from the ChIP-Atlas (57). (**D**) Schematic representation of combination of RT-qPCR and RT-PCR/amplicon-seq for quantitative analysis of allelic expression. (**E**) Quantitative analysis of *Meg3* and *Mirg* allelic expression on D7. Expression is shown relative to scr gRNA-transfected cells. (**F**) Schematic representation of combination of ChIP-qPCR and ChIP-PCR/amplicon-seq for quantitative analysis of allelic histone modifications. (**G–J**) Quantitative analysis of allelic histone modifications, H3K4me3 (**G**) and H3K27ac (**H**). Anti-pan-histone H3 antibody (**I**) and IgG (**J**) were used as experimental controls. For all panels, asterisks indicate statistically significant differences compared to the scr control by unpaired Student's *t* test (*n* = 3). Asterisks in parentheses indicate significance for the paternal allele: *$P < 0.05$, **$P < 0.01$, ***$P < 0.001$. Error bars represent ± SD. See also Supplementary Figure S1.

Ch1–3) and *Meg3*-DMR (PCR primer set; Ch6) were significantly elevated in cells transfected with gR2 compared to controls transfected with scr gRNA, and these elevations were derived from the paternal allele on which both H3K4me3 and H3K27ac were depleted in normal ESCs (Figure 2G, H). The combination of ChIP-qPCR and ChIP-PCR/amplicon-seq analysis using pan-histone H3 antibody showed an approximately 1:1 ratio between B6 and JF1 alleles, indicating the methodological relevance of this assay (Figure 2I). IgG was used as a negative control for the ChIP-qPCR experiment (Figure 2J).

These results indicate that induced DNA hypomethylation at paternal IG-DMR-Rep maternalised the paternal allele in terms of expression of *Meg3* and *Mirg* and histone modifications at IG- and *Meg3*-DMRs.

Loss of DNA methylation at IG-DMR-Rep is maintained through neuronal differentiation

To investigate whether induced hypomethylation at IG-DMR-Rep by gR2 is maintained through differentiation, we induced the differentiation of ESCs transfected with the DNA demethylation tool along with scr or gR2 gRNA into neural precursors based on the SFEB method (31) (Figure 3A). In addition, as neuronal differentiation upregulates three paternally expressed genes in this domain (i.e. *Dlk1*, *Rtl1* and *Dio3*) although they are below the limit of detection in undifferentiated ESCs, their expression levels were also measured in differentiated neuronal cells. Cells on D7 or later were differentiated, which was confirmed by their neurite-like morphology and expression of marker genes (pluripotency markers, *Oct4* and *Nanog*; and neuroectodermal marker, *Sox1*) (Figure 3B). Control cells transfected with scr gRNA as well as NTF cells gained DNA methylation on maternal Bi1 and Bi3 sites during neuronal differentiation (Figure 3C and Supplementary Figure S3). These observations are consistent with a previous study reporting gain of methylation on maternal IG-DMR in neural stem cells and astrocytes *in vivo* (38). The level of DNA methylation of paternal IG- and *Meg3*-DMRs in cells transfected with gR2 was significantly lower than those of control cells transfected with scr gRNA or NTF cells (Figure 3C and Supplementary Figure S3). Expression levels of three maternally expressed genes, i.e. *Meg3*, *Meg8*, and *Mirg*, were significantly upregulated from the paternal allele, while the paternally expressed genes, *Dlk1*, *Rtl1* and *Dio3*, were significantly downregulated (Figure 3D). In this analysis, we measured DNA methylation level at *Meg8*-DMR, which is located in intron 2 of *Meg8* and is, in contrast to IG- and *Meg3*-DMRs, hypermethylated on the maternal allele and hypomethylated on the paternal allele in embryonic day 19 (E19) fetal tissues (39) (Supplementary Figure S2A, B). The methylation level was higher on paternal *Meg8*-DMR of gR2-transfected cells than scr gRNA-transfected cells or NTF cells (Figure 3C and Supplementary Figure S3). These results indicate that induced DNA hypomethylation at IG-DMR-Rep by transient expression of the demethylation tool persisted through differentiation, and that the hypomethylated paternal allele behaved like its counterpart maternal allele in neuronal precursor cells.

Gain of DNA methylation at IG-DMR-Rep showed inverse effects to the loss of DNA methylation

In addition to the loss of methylation, we performed a gain of methylation experiment using a DNA methylation tool consisting of pX330-based dCas9GCN4-P2A-Puro and scFvGCN4sfGFPDNMT3A (Figure 1A). To assess gRNA-independent off-target methylation activity, we transfected the scr gRNA with the methylation tool into BJ ESCs, and found a small effect on DNA methylation at IG- and *Meg3*-DMRs on D3 and D7 (Figure 4A and Supplementary Figure S4A). Next, we checked the functionality of the gRNAs by measuring DNA methylation levels on D3. By comparing the DNA methylation levels at the gRNA target sites between cells transfected with each gRNA and the scr gRNA, we confirmed that gRNAs other than gR5 induced hypermethylation (Figure 4B and Supplementary Figure S4B). Therefore, we used gR7 to target IG^{TRE} instead of gR5 for the subsequent targeted DNA methylation experiment. On D7, the cells transfected with gR2 showed more than 40% DNA hypermethylation on the maternal allele at all sites in IG-DMR and 30% in *Meg3*-DMR, and about 2-fold higher level for both alleles at the Bi4 site compared to cells transfected with scr gRNA (Figure 4C and Supplementary Figure S4C). The cells transfected with gR1 and gR3 also showed higher methylation levels compared to the control cells transfected with scr gRNA, whereas the cells transfected with gR7 or gR4 relapsed to similar levels to those transfected with scr gRNA. The cells transfected with gR6 retained hypermethylation at *Meg3*-DMR on D7 but showed no effect on IG-DMR methylation. Consistent with the induced hypermethylation by gR2, the binding of ZFP57 on the maternal allele at the Bi2 site was significantly increased, as revealed by the combination of ChIP-qPCR and ChIP-PCR/amplicon-seq (Figures 2F and 4D).

On D7, the cells transfected with gR2 showed decreased expression of *Meg3* (20.4%, $P = 0.036$) compared to cells transfected with scr gRNA (Figure 4E). DNA methylation at *Meg3*-DMR was maintained at a higher level in the cells transfected with gR6, but the *Meg3* expression level was not altered (Figures 2E and 4E).

Histone modifications were investigated in cells transfected with gR2 on D7 by the combination of ChIP-qPCR and ChIP-PCR/amplicon-seq (Figure 2F). H3K4me3 was significantly decreased in IG- and *Meg3*-DMRs compared to NTF cells or cells transfected with scr gRNA (Figure 4F). By contrast, H3K9me3 on the maternal allele was markedly increased at IG- and *Meg3*-DMRs (Figure 4G). The pan-histone H3 antibody and IgG were used as experimental controls for the combination of ChIP-qPCR and ChIP-PCR/amplicon-seq (Figure 4H, I).

Finally, we induced ESCs transfected with gR2 or scr gRNA on D7 or later to differentiate into neural precursors (Figures 3A and 5A). The cells transfected with gR2 showed a significantly higher level of DNA methylation on maternal IG- (Bi1, Bi2, Bi3 and Bi5 sites) and *Meg3*-DMRs (Bi6 site), and the total level for both alleles (Bi4 site) compared to cells transfected with scr gRNA (Figure 5B and Supplementary Figure S5). The maternal *Meg8*-DMR of cells transfected with gR2 showed a lower level of DNA methylation compared to cells transfected with scr gRNA
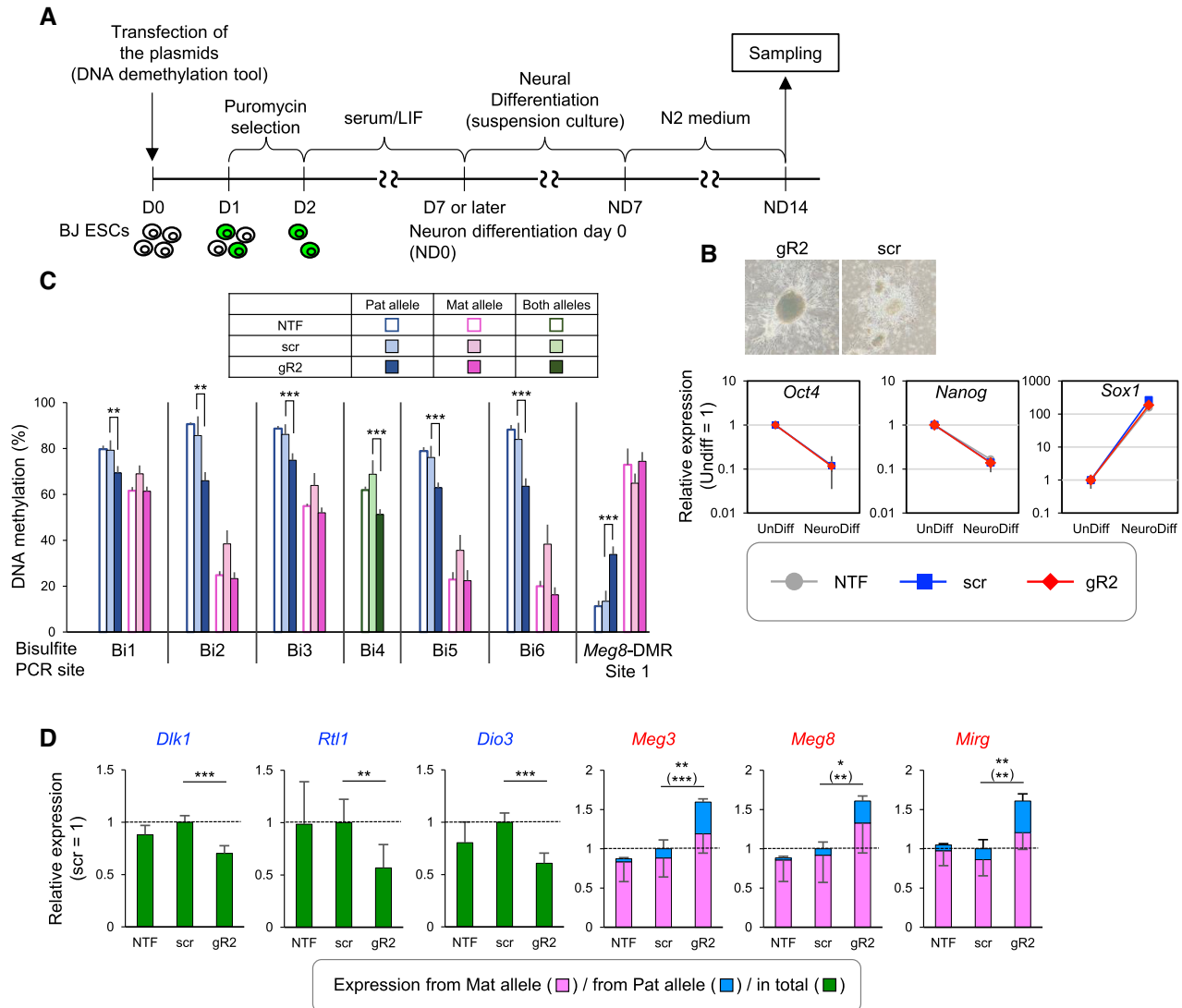
Figure 3. Effects of targeted loss of DNA methylation persists through neuronal differentiation. (**A**) Experimental scheme for DNA methylation editing followed by induction of neuronal differentiation. ND: days after induction of neuronal differentiation. (**B**) Successful neuronal differentiation was confirmed by cellular morphology, and expression of marker genes. (**C**) DNA methylation levels at IG- (Bi1–5), *Meg3*- (Bi6) and *Meg8*-DMRs in scr gRNA and gR2-transfected cells on ND14. Paternal and maternal alleles were separated except for Bi4. (**D**) Quantitative analysis of allelic expression of genes in the *Dlk1-Dio3* imprinted domain. Expression is shown relative to scr gRNA-transfected cells. For all panels, asterisks indicate statistically significant differences compared to scr controls by unpaired Student's *t* test ($n = 6$, see MATERIALS AND METHODS for details). Asterisks in parentheses indicate significance for the paternal allele: $*P < 0.05$, $**P < 0.01$, $***P < 0.001$. Error bars represent ± SD. See also Supplementary Figures S2 and S3.

(Figure 5B and Supplementary Figure S5). We investigated the expression levels and alleles of the genes in the domain by the combination of RT-qPCR and RT-PCR/amplicon-seq (Figure 2D). Three paternally expressed genes (*Dlk1*, *Rtl1*, and *Dio3*) showed significant upregulation due to expression from the maternal allele, whereas three maternally expressed genes (*Meg3*, *Meg8* and *Mirg*) showed significant downregulation in cells transfected with gR2 compared to cells transfected with scr gRNA (Figure 5C). Interestingly, *Rtl1* from the paternal allele also showed 1.5-fold upregulation in cells transfected with gR2 ($P = 0.07$, $n = 6$). As its maternally expressed antisense transcript, *Rtl1as*, encodes seven microRNAs that degrade *Rtl1* through RNA interference (RNAi), it is suggested that *Rtl1as* was also down-

regulated by gR2-targeted gain of DNA methylation (8,34). Taken together, these observations indicate that the gain of DNA methylation at IG-DMR-Rep by gR2 caused paternalisation of the maternal allele and showed inverse effects against the effects caused by loss of DNA methylation at IG-DMR-Rep.

DISCUSSION

DNA methylation is considered to be a pivotal component of gene regulation in combination with other epigenetic modifications, such as histone modifications. The role of DNA methylation has been investigated by mutating factors associated with the regulation of DNA methyla-
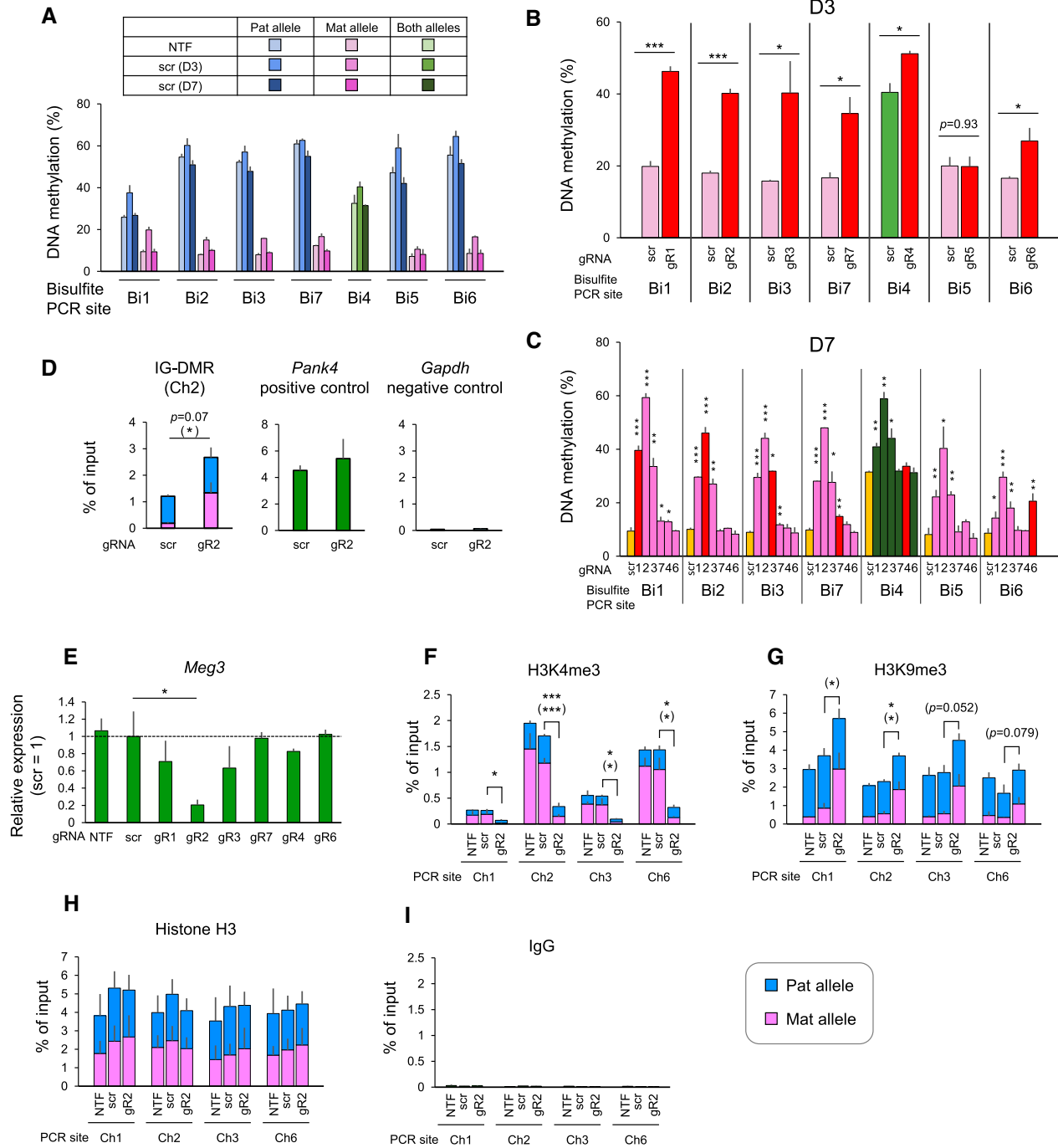
Figure 4. Effects of targeted gain of DNA methylation at IG- and *Meg3*-DMRs. (**A**) DNA methylation levels at IG-DMR (Bi1–5, and Bi7) and *Meg3*-DMR (Bi6) in NTF and scr gRNA-transfected BJ ESCs on D3 and D7. Paternal and maternal alleles were separated except for Bi4. (**B**) DNA methylation levels of cells transfected with one of the gRNAs (scr or gR1–gR7) at each gRNA target site on D3. DNA methylation levels of the maternal allele are shown except for the Bi4 site, which is shown for both alleles. (**C**) DNA methylation levels on D7. DNA methylation levels of the maternal allele are shown except for the Bi4 site, which is shown for both alleles. Yellow bars indicate scr gRNA and red bars indicate gRNAs targeting the bisulfite-PCR sites. (**D**) Quantitative analysis of allelic ZFP57 binding by combination of ChIP-qPCR and ChIP-PCR/amplicon-seq at the Ch2 site in IG-DMR. Genomic loci of *Pank4* and *Gapdh* that were not targeted by the guide RNAs were used as positive and negative controls, respectively (37). (**E**) Quantitative expression of *Meg3* on D7. Expression is shown relative to scr gRNA-transfected cells. (**F–I**) Quantitative analysis of allelic histone modifications, H3K4me3 (**F**) and H3K9me3 (**G**). Anti-pan-histone H3 antibody (**H**) and IgG (**I**) were used as experimental controls. For all panels, asterisks indicate statistically significant differences compared to scr controls by unpaired Student's *t* test (*n* = 3). Asterisks in parentheses indicate significance for maternal allele: **P* < 0.05, ***P* < 0.01, ****P* < 0.001. Error bars represent ± SD. See also Supplementary Figure S4.
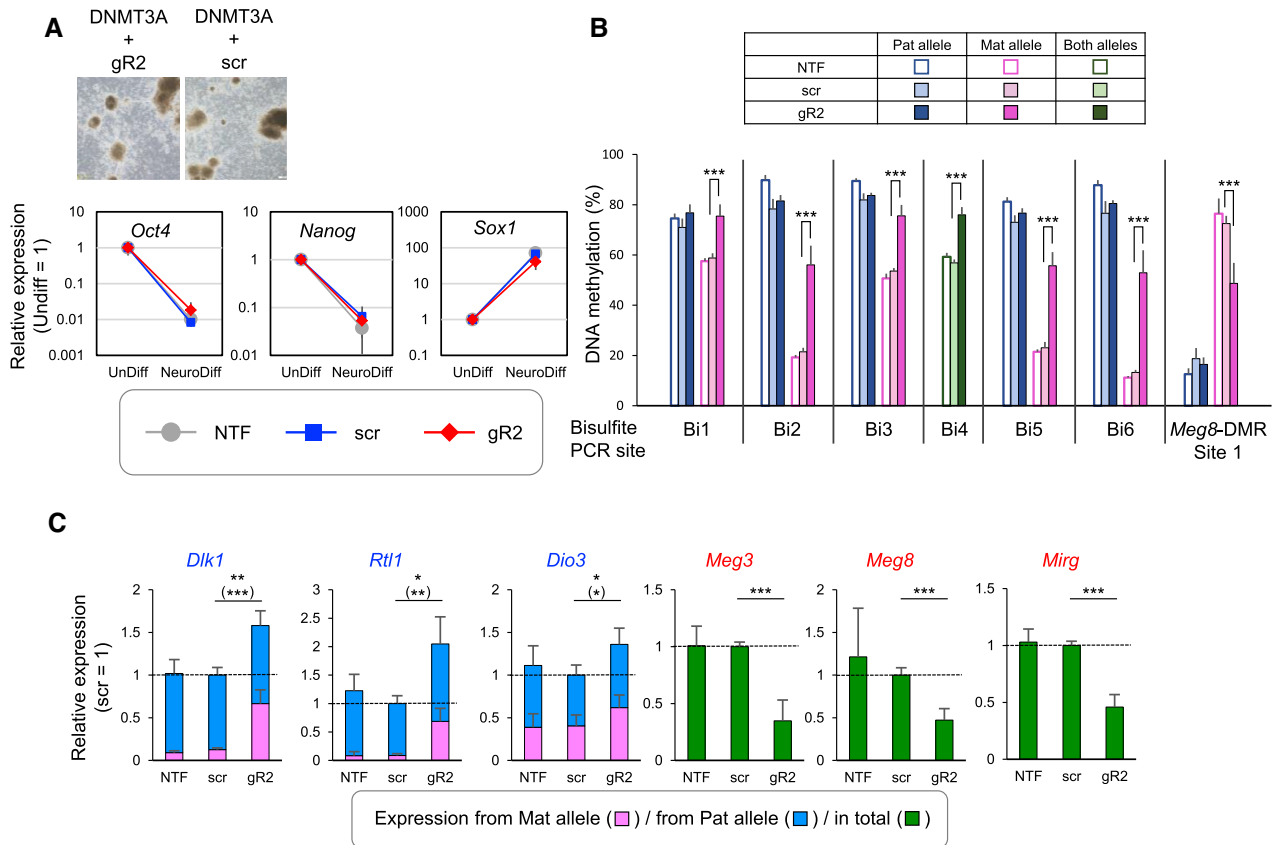
Figure 5. Effects of targeted gain of DNA methylation persists through neuronal differentiation. (**A**) Successful neuronal differentiation was confirmed by cellular morphology, and expression of marker genes. ND: days after induction of neuronal differentiation. (**B**) DNA methylation levels at IG- (Bi1–5), *Meg3*- (Bi6), and *Meg8*-DMRs in scr gRNA- and gR2-transfected cells on ND14. Paternal and maternal alleles were separated except for Bi4. (**C**) Quantitative analysis of allelic expression of genes in the *Dlk1-Dio3* imprinted domain. Expression is shown relative to scr gRNA-transfected cells. For all panels, asterisks indicate statistically significant differences compared to scr controls by unpaired Student's *t* test ($n = 6$, see MATERIALS AND METHODS for details). Asterisks in parentheses indicate significance for the maternal allele: $*P < 0.05$, $**P < 0.01$, $***P < 0.001$. Error bars represent ± SD. See also Supplementary Figure S5.

tion, such as DNA methyltransferases, or by deleting genomic elements whose DNA methylation state is changed during cell differentiation/development or in disease. However, mutating factors change the genome-wide epigenetic state, and deleting genomic elements affects not only DNA methylation but also other epigenetic modifications or the state of DNA binding factors. Therefore, it has been difficult to provide direct evidence of how DNA methylation at a specific locus functions (25). In this study, we applied CRISPR/Cas9-based DNA methylation editing tools, and performed both gain and loss of DNA methylation experiments at the *Dlk1-Dio3* imprinted domain. Importantly, as we introduced the DNA methylation editing tools transiently and used catalytically inactive TET1 as a control, we could exclude the possibility that the observed effects were due to interference with binding of endogenous proteins by occupation of gRNA target sites by dCas9. Therefore, our results provide evidence of the role of DNA methylation per se. Another important finding is that one gRNA targeting IG-DMR-Rep was sufficient to affect the entirety of the *Dlk1-Dio3* imprinted domain spanning approximately 860 kb, and that the effect persisted for a long period, even through cell dif-

ferentiation, thus representing a core DNA methylation site.

Considering the results of both the loss and gain of DNA methylation experiments, it is clear that the DNA methylation state at IG-DMR-Rep spreads into the entirety of the IG-DMR, and hypomethylated IG^{TRE} functions as an enhancer of *Meg3*, while methylated IG^{TRE} does not (Figure 6). On the other hand, hypo- or hypermethylation induced at IG^{TRE} by gR4/gR7 or gR5 did not persist until D7 or alter the DNA methylation at *Meg3*-DMR, suggesting that DNA methylation at IG^{TRE} is associated with enhancer activity for *Meg3*, but not with epigenetic regulation of the *Dlk1-Dio3* domain (Supplementary Table S1). It has been suggested that *Meg3* mRNA functions as a cofactor for polycomb repressive complex 2 (PRC2) to direct PRC2 to the *Dlk1* promoter, and they suppress *Dlk1 in cis* (40). Taken together, these results indicate that DNA methylation state at IG-DMR-Rep is a *bona fide* element to determine of whether the allele behaves as the intrinsic maternal or paternal allele.

Further study is needed to elucidate the function of DNA methylation at *Meg3*-DMR. Although lower and higher DNA methylation at *Meg3*-DMR induced by gR6 were
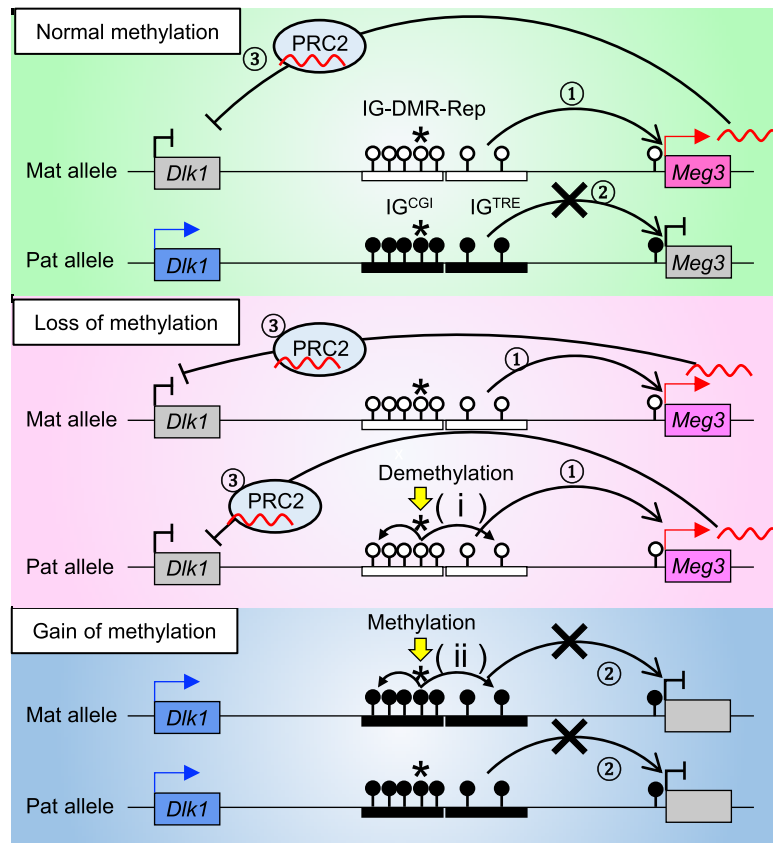
Figure 6. A model for imprinted regulation by DNA methylation state at IG-DMR-Rep. In normal ESCs, hypomethylated maternal IG^{TRE} functions as an enhancer to activate *Meg3* transcription (①), whereas hypermethylated paternal IG^{TRE} does not (②). The transcribed *Meg3* mRNA is incorporated into PRC2 to direct PRC2 to *Dlk1* and suppress it *in cis* (③) (40). When the hypermethylated paternal IG-DMR-Rep is demethylated (i), the entire IG-DMR is hypomethylated and *Meg3* is derepressed on the paternal allele. By contrast, when the hypomethylated maternal IG-DMR-Rep is methylated (ii), the entire IG-DMR is hypermethylated and maternal *Meg3* is repressed, and *Dlk1* is expressed biallelically. Filled circle: methylated CpG; open circle: unmethylated CpG; asterisk: IG-DMR-Rep.

maintained at D7, mono allelic expression and the expression level of *Meg3* were unaffected in both cases (Supplementary Table S1). In the *Gtl2^lacZ* mouse model, in which the *LacZ* transgene (TG) was inserted approximately 1-kb upstream of *Meg3*-DMR (Supplementary Figure S6), paternal transmission of the TG induced almost complete demethylation of the paternal *Meg3*-DMR without affecting IG-DMR, and partial derepression of paternal *Meg3*, suggesting some functions of DNA methylation at *Meg3*-DMR (22). Stronger DNA methylation editing, i.e. almost complete demethylation and methylation, is needed to draw conclusions regarding the function of DNA methylation at *Meg3*-DMR.

MEG8-DMR was first reported in the human genome (39,41). On analysing the orthologous region of the mouse genome, we found maternally hypermethylated and paternally hypomethylated *Meg8*-DMR in intron 2 of *Meg8* in mouse fetal tissues (Supplementary Figure S2). Analysis of human KOS patients with several genomic deletions suggested that establishment of DNA methylation at *MEG8*-DMR requires transcription from *MEG3* to *MEG8* (39). This may also be the case in mice. Intriguingly, we found that *Meg8*-DMR includes a peak in the ChIP-seq for CTCF in mouse ESCs (Supplementary Figure S2). Because CTCF

is a DNA methylation-sensitive DNA binding protein, it is possible that CTCF only binds the hypomethylated paternal *Meg8*-DMR, and contributes to allele-specific chromatin conformation. Additionally, we noticed that *Meg8*-DMR is located 2.5-kb upstream of one of the alternative leader exons of *Rtl1* (*Rtl1*-Ex1b) (42) (Supplementary Figure S2). These observations suggest that *Meg8*-DMR may function in *Rtl1* regulation through chromatin conformation, or as a *cis*-regulatory element such as a promoter or enhancer. Because misregulation of *Rtl1* is one of the main causes of KOS and TS, a deletion experiment of *Meg8*-DMR would be instructive (8,43,44).

The molecular mechanism by which the DNA methylation state at IG-DMR-Rep spreads throughout the entire IG-DMR is also intriguing. As IG-DMR-Rep contains a tandem repeat of ZFP57 binding sequences, ZFP57, which binds to methylated DNA, would be a key player in this mechanism (16,45–47). ZFP57 can act as a scaffold for the KAP1 complex, which contains KAP1 (also known as TRIM28), CBX1/3/5 and SUMO1/2. This complex recruits other factors, such as DNA methyltransferases (DNMT1 and DNMT3A), histone H3K9 methyltransferase (SETDB1) and its associated protein, ATF7IP, as well as the NuRD chromatin remodelling complex con-

taining methylated DNA binding protein (MBD3), histone H3–K4 demethylase (KDM1A, also known as LSD1), and histone deacetylase (CHD4) (48–50). Indeed, publicly available ChIP-seq data show that these factors bind IG-DMR-Rep in ESCs or induced pluripotent stem cells (Supplementary Figure S6). Also, ZFP57 is essential for maintenance of DNA methylation at imprinted DMRs (5,51). These observations, in addition to our results, suggest that changes in the binding state of ZFP57 at IG-DMR-Rep can be a starting point for shifting the epigenetic state of the entire IG-DMR. On the other hand, the mechanism by which DNA methylation state at IG-DMR affects *Meg3*-DMR would be associated with chromatin loop formation, as proposed previously (16,19), and factors associated with loop formation (CTCF, YY1, SMC1A, STAG1/2, RAD21 and ZFP143) bind IG- and *Meg3*-DMRs (52) (Supplementary Figure S6).

Recent genetic modification experiments have shown that paternal methylated IG-DMR-Rep is essential for preserving the imprinting state at this domain *in vivo* (4,17). In addition, Aronson *et al.* (2021) showed that IG-DMR is a bipartite element consisting of IG^{CGI}, which contains IG-DMR-Rep, and IG^{TRE} which functions as an enhancer of *Meg3 in vitro*. Our results indicate that the DNA methylation states at IG-DMR-Rep, regardless of whether it is methylated or unmethylated, spread into adjacent IG^{TRE}, and affect the imprinted expression of the genes throughout the domain. Therefore, we argue that DNA methylation at IG-DMR-Rep is a real core element for epigenetic regulation in the 3.8 kb IG-DMR, so that means the whole of the *Dlk1-Dio3* imprinted domain. Notably, we found that the hypermethylation at IG^{TRE} induced by gR7 or gR5 did not persist, and therefore, did not alter the imprinting state of the domain, including imprinted *Meg3* expression and DNA methylation at IG- and *Meg3*-DMRs. Aronson *et al.* (2021) also performed DNA methylation editing using dCas9-TET1CD and DNMT3A direct fusion proteins. The differences between their strategy and that used herein are as follows: they introduced tools in a stable manner using a lentiviral vector, compared with the transient expression conducted in the present study; furthermore, they introduced multiple gRNAs simultaneously, whereas we introduced a single gRNA at a time. Consistent with their observation, we observed a spread of hypomethylation into whole of the IG-DMR and *Meg3*-DMR when IG^{CGI} was demethylated. On the other hand, they reported that inducing DNA methylation at IG^{TRE} increased DNA methylation at maternal IG- and *Meg3*-DMRs, and decreased the *Meg3* expression level, which is inconsistent with our results. We speculate that this may have been because the lentiviral-transduced dCas9-DNMT3A protein in their experiment remained on the maternal IG^{TRE} and sterically interfered with binding of transcription factors (e.g. AFF3 and ZFP281) that are necessary to activate the enhancer function for *Meg3*, and the repressed *Meg3* expression led to hypermethylation at maternal *Meg3*-DMR (20,21). It is also suggested that steric hindrance caused by stable expression of Cas9-related artificial proteins triggers epigenetic alterations by interfering with the binding of endogenous proteins at target sites, which could be the cause of the spread of DNA methylation into IG^{CGI} in their experiment (53). Fur-

ther studies with stable expression of catalytically inactive dCas9-TET1CD or dCas9-DNMT3A with gRNAs targeting IG^{TRE} are required to resolve this discrepancy.

The methodologies used in this study, i.e. the bisulfite-PCR/amplicon-seq, the combination of RT-qPCR and RT-PCR/amplicon-seq, and ChIP-qPCR and ChIP-PCR/amplicon-seq, provide robust data for genomic imprinting analysis, and are cost effective and highly quantitative compared to conventional strategies, such as bisulfite-sequencing through TA-cloning, and RT-PCR followed by restriction fragment length polymorphism (RFLP) assay. Bisulfite-PCR/amplicon-seq enables the simultaneous reading large numbers of samples (>100 samples, limited by the number of indexes, but no limitation for PCR primer sets). Compared to pyrosequencing or whole-genome bisulfite sequencing, this strategy has advantages in terms of read length of each amplicon (300–500 bp, which is similar to the conventional bisulfite-PCR-sequencing strategy), and each CpG methylation in each molecule can be observed, which is informative particularly for genomic imprinting research (Supplementary Figures S1–S5). The high degree of quantitativeness of the combination strategy of RT-qPCR and RT-PCR/amplicon-seq to measure allelic expression was confirmed using BJ genomic DNA as the template for PCR, in which SNPs specific to the maternal or paternal allele were detected at almost 1:1 ratio (Supplementary Data 2, related to Figure 3A). Similarly, the relevance of the combination of ChIP-qPCR and ChIP-PCR/amplicon-seq was confirmed by experiments using anti-histone H3 antibody, in which paternal and maternal alleles were detected at almost 1:1 ratio (Figures 2I and 4H). This strategy would be more suitable than the costly ChIP-seq analysis for investigation of limited regions with large numbers of samples.

Although we carefully controlled each experiment by comparison with the effects of scr gRNA or NTF samples, imprinted DMRs are susceptible to *in vitro* ESC culture conditions (54–56). It is also necessary to consider that DNA methylation editing in ESCs is not perfect i.e. some of the cells in both the loss and gain of DNA methylation experiments retained the normal DNA methylation states. In addition to these experimental limitations using ESCs, it should be noted that IG-DMR is the causative region of human KOS and TS, and that some patients show epimutations, such as hyper- or hypomethylation, at IG-DMR (9,23,24). Therefore, *in vivo* experimental systems with introduction of DNA methylation editing tools into early mouse embryos would be important to explore whether we can achieve complete DNA methylation editing in the whole body and cause the phenotypes associated with KOS and TS.

Despite these limitations, we confirmed the power of the DNA methylation editing tools combining CRISPR/Cas9 and SunTag systems (27,28). These tools enable us to study the causative role of DNA methylation in gene expression at specific sites, which can be referred to as 'reverse epigenetics' (this term comes from the term 'reverse genetics'). Our study presents a reverse epigenetics model to explore whether core DNA methylation similar to IG-DMR-Rep exists in other ICRs as well as *cis*-regulatory DNA elements (e.g. enhancers).

REFERENCES

1. Tucci,V., Isles,A.R., Kelsey,G., Ferguson-Smith,A.C., Bartolomei,M.S., Benvenisty,N., Bourc'his,D., Charalambous,M., Dulac,C., Feil,R. *et al.* (2019) Genomic imprinting and physiological processes in mammals. *Cell*, **176**, 952–965.
2. Yoon,B.J., Herman,H., Sikora,A., Smith,L.T., Plass,C. and Soloway,P.D. (2002) Regulation of DNA methylation of Rasgrf1. *Nat. Genet.*, **30**, 92–96.
3. Lewis,A., Mitsuya,K., Constancia,M. and Reik,W. (2004) Tandem repeat hypothesis in imprinting: deletion of a conserved direct repeat element upstream of H19 has no effect on imprinting in the Igf2-H19 region. *Mol. Cell. Biol.*, **24**, 5650–5656.
4. Saito,T., Hara,S., Kato,T., Tamano,M., Muramatsu,A., Asahara,H. and Takada,S. (2018) A tandem repeat array in IG-DMR is essential for imprinting of paternal allele at the Dlk1-Dio3 domain during embryonic development. *Hum. Mol. Genet.*, **27**, 3283–3292.
5. Li,X., Ito,M., Zhou,F., Youngson,N., Zuo,X., Leder,P. and Ferguson-Smith,A.C. (2008) A maternal-zygotic effect gene, Zfp57, maintains both maternal and paternal imprints. *Dev. Cell*, **15**, 547–557.
6. Takahashi,N., Coluccio,A., Thorball,C.W., Planet,E., Shi,H., Offner,S., Turelli,P., Imbeault,M., Ferguson-Smith,A.C. and Trono,D. (2019) ZNF445 is a primary regulator of genomic imprinting. *Genes Dev*, **33**, 49–54.
7. Monteagudo-Sánchez,A., Hernandez Mora,J.R., Simon,C., Burton,A., Tenorio,J., Lapunzina,P., Clark,S., Esteller,M., Kelsey,G., López-Siguero,J.P. *et al.* (2020) The role of ZFP57 and additional KRAB-zinc finger proteins in the maintenance of human imprinted methylation and multi-locus imprinting disturbances. *Nucleic Acids Res.*, **48**, 11394–11407.
8. Sekita,Y., Wagatsuma,H., Nakamura,K., Ono,R., Kagami,M., Wakisaka,N., Hino,T., Suzuki-Migishima,R., Kohda,T., Ogura,A. *et al.* (2008) Role of retrotransposon-derived imprinted gene, Rtl1, in the feto-maternal interface of mouse placenta. *Nat. Genet.*, **40**, 243–248.
9. Kagami,M., Sekita,Y., Nishimura,G., Irie,M., Kato,F., Okada,M., Yamamori,S., Kishimoto,H., Nakayama,M., Tanaka,Y. *et al.* (2008) Deletions and epimutations affecting the human 14q32.2 imprinted region in individuals with paternal and maternal upd(14)-like phenotypes. *Nat. Genet.*, **40**, 237–242.
10. Takahashi,N., Okamoto,A., Kobayashi,R., Shirai,M., Obata,Y., Ogawa,H., Sotomaru,Y. and Kono,T. (2009) Deletion of Gtl2, imprinted non-coding RNA, with its differentially methylated region induces lethal parent-origin-dependent defects in mice. *Hum. Mol. Genet.*, **18**, 1879–1888.
11. Hernandez,A., Martinez,M.E., Fiering,S., Galton,V.A. and St. Germain,D. (2006) Type 3 deiodinase is critical for the maturation and function of the thyroid axis. *J. Clin. Invest.*, **116**, 476–484.
12. Moon,Y.S., Smas,C.M., Lee,K., Villena,J.A., Kim,K.-H., Yun,E.J. and Sul,H.S. (2002) Mice lacking paternally expressed Pref-1/Dlk1 display growth retardation and accelerated adiposity. *Mol. Cell. Biol.*, **22**, 5585–5592.
13. Zhou,Y., Cheunsuchon,P., Nakayama,Y., Lawlor,M.W., Zhong,Y., Rice,K.A., Zhang,L., Zhang,X., Gordon,F.E., Lidov,H.G.W. *et al.* (2010) Activation of paternally expressed genes and perinatal death caused by deletion of the Gtl2 gene. *Development*, **137**, 2643–2652.
14. Takada,S., Paulsen,M., Tevendale,M., Tsai,C.E., Kelsey,G., Cattanach,B.M. and Ferguson-Smith,A.C. (2002) Epigenetic analysis of the Dlk1-Gtl2 imprinted domain on mouse chromosome 12: implications for imprinting control from comparison with Igf2-H19. *Hum. Mol. Genet.*, **11**, 77–86.
15. Lin,S.P., Youngson,N., Takada,S., Seitz,H., Reik,W., Paulsen,M., Cavaille,J. and Ferguson-Smith,A.C. (2003) Asymmetric regulation of imprinting on the maternal and paternal chromosomes at the Dlk1-Gtl2 imprinted cluster on mouse chromosome 12. *Nat. Genet.*, **35**, 97–102.
16. Aronson,B.E., Scourzic,L., Shah,V., Swanzey,E., Kloetgen,A., Polyzos,A., Sinha,A., Azziz,A., Caspi,I., Li,J. *et al.* (2021) A bipartite element with allele-specific functions safeguards DNA methylation imprints at the Dlk1-Dio3 locus. *Dev. Cell*, **56**, 3052–3065.
17. Hara,S., Terao,M., Muramatsu,A. and Takada,S. (2019) Efficient production and transmission of CRISPR/Cas9-mediated mutant alleles at the IG-DMR via generation of mosaic mice using a modified 2CC method. *Sci. Rep.*, **9**, 20202.
18. Paulsen,M., Takada,S., Youngson,N.A., Benchaib,M., Charlier,C., Segers,K., Georges,M. and Ferguson-Smith,A.C. (2001) Comparative sequence analysis of the imprinted Dlk1-Gtl2 locus in three mammalian species reveals highly conserved genomic elements and refines comparison with the Igf2-H19 region. *Genome Res.*, **11**, 2085–2094.
19. Das,P.P., Hendrix,D.A., Apostolou,E., Buchner,A.H., Canver,M.C., Beyaz,S., Ljuboja,D., Kuintzle,R., Kim,W., Karnik,R. *et al.* (2015) PRC2 is required to maintain expression of the maternal Gtl2-Rian-Mirg locus by preventing de novo DNA methylation in mouse embryonic stem cells. *Cell Rep.*, **12**, 1456–1470.
20. Luo,Z., Lin,C., Woodfin,A.R., Bartom,E.T., Gao,X., Smith,E.R. and Shilatifard,A. (2016) Regulation of the imprinted Dlk1-Dio3 locus by allele-specific enhancer activity. *Genes Dev.*, **30**, 92–101.
21. Wang,Y., Shen,Y., Dai,Q., Yang,Q., Zhang,Y., Wang,X., Xie,W., Luo,Z. and Lin,C. (2017) A permissive chromatin state regulated by ZFP281-AFF3 in controlling the imprinted Meg3 polycistron. *Nucleic Acids Res.*, **45**, 1177–1185.
22. Sekita,Y., Wagatsuma,H., Irie,M., Kobayashi,S., Kohda,T., Matsuda,J., Yokoyama,M., Ogura,A., Schuster-Gossler,K., Gossler,A. *et al.* (2006) Aberrant regulation of imprinted gene expression in Gtl2lacZ mice. *Cytogenet. Genome Res.*, **113**, 223–229.
23. Kagami,M., Matsuoka,K., Nagai,T., Yamanaka,M., Kurosawa,K., Suzumori,N., Sekita,Y., Miyado,M., Matsubara,K., Fuke,T. *et al.* (2012) Paternal uniparental disomy 14 and related disorders: placental gene expression analyses and histological examinations. *Epigenetics*, **7**, 1142–1150.
24. Kagami,M., Kurosawa,K., Miyazaki,O., Ishino,F., Matsuoka,K. and Ogata,T. (2015) Comprehensive clinical studies in 34 patients with molecularly defined UPD(14)pat and related conditions (Kagami-Ogata syndrome). *Eur. J. Hum. Genet.*, **23**, 1488–1498.
25. Nakamura,M., Gao,Y., Dominguez,A.A. and Qi,L.S. (2021) CRISPR technologies for precise epigenome editing. *Nat. Cell Biol.*, **23**, 11–22.

26. Konermann,S., Brigham,M.D., Trevino,A.E., Joung,J., Abudayyeh,O.O., Barcena,C., Hsu,P.D., Habib,N., Gootenberg,J.S., Nishimasu,H. *et al.* (2015) Genome-scale transcriptional activation by an engineered CRISPR-Cas9 complex. *Nature*, **517**, 583–588.

27. Morita,S., Noguchi,H., Horii,T., Nakabayashi,K., Kimura,M., Okamura,K., Sakai,A., Nakashima,H., Hata,K., Nakashima,K. *et al.* (2016) Targeted DNA demethylation in vivo using dCas9-peptide repeat and scFv-TET1 catalytic domain fusions. *Nat. Biotechnol.*, **34**, 1060–1065.

28. Pflueger,C., Tan,D., Swain,T., Nguyen,T., Pflueger,J., Nefzger,C., Polo,J.M., Ford,E. and Lister,R. (2018) A modular dCas9-SunTag DNMT3A epigenome editing system overcomes pervasive off-target activity of direct fusion dCas9-DNMT3A constructs. *Genome Res.*, **28**, 1193–1206.

29. Yagi,M., Kishigami,S., Tanaka,A., Semi,K., Mizutani,E., Wakayama,S., Wakayama,T., Yamamoto,T. and Yamada,Y. (2017) Derivation of ground-state female ES cells maintaining gamete-derived DNA methylation. *Nature*, **548**, 224–227.

30. Choi,J., Huebner,A.J., Clement,K., Walsh,R.M., Savol,A., Lin,K., Gu,H., Di Stefano,B., Brumbaugh,J., Kim,S.Y. *et al.* (2017) Prolonged Mek1/2 suppression impairs the developmental potential of embryonic stem cells. *Nature*, **548**, 219–223.

31. Watanabe,K., Kamiya,D., Nishiyama,A., Katayama,T., Nozaki,S., Kawasaki,H., Watanabe,Y., Mizuseki,K. and Sasai,Y. (2005) Directed differentiation of telencephalic precursors from embryonic stem cells. *Nat. Neurosci.*, **8**, 288–296.

32. Cong,L., Ran,F.A., Cox,D., Lin,S., Barretto,R., Habib,N., Hsu,P.D., Wu,X., Jiang,W., Marraffini,L.A. *et al.* (2013) Multiplex genome engineering using CRISPR/Cas systems. *Science*, **339**, 819–823.

33. Sekita,Y., Sugiura,Y., Matsumoto,A., Kawasaki,Y., Akasaka,K., Konno,R., Shimizu,M., Ito,T., Sugiyama,E., Yamazaki,T. *et al.* (2021) AKT signaling is associated with epigenetic reprogramming via the upregulation of TET and its cofactor, alpha-ketoglutarate during iPSC generation. *Stem Cell Res. Ther.*, **12**, 510.

34. Davis,E., Caiment,F., Tordoir,X., Cavaillé,J., Ferguson-Smith,A.C., Cockett,N., Georges,M. and Charlier,C. (2005) RNAi-mediated allelic trans-interaction at the imprinted Rtl1/Peg11 locus. *Curr. Biol.*, **15**, 743–749.

35. Fujita,T., Asano,Y., Ohtsuka,J., Takada,Y., Saito,K., Ohki,R. and Fujii,H. (2013) Identification of telomere-associated molecules by engineered DNA-binding molecule-mediated chromatin immunoprecipitation (enChIP). *Sci. Rep.*, **3**, 3171.

36. Kobayashi,H., Suda,C., Abe,T., Kohara,Y., Ikemura,T. and Sasaki,H. (2006) Bisulfite sequencing and dinucleotide content analysis of 15 imprinted mouse differentially methylated regions (DMRs): paternally methylated DMRs contain less CpGs than maternally methylated DMRs. *Cytogenet. Genome Res.*, **113**, 130–137.

37. Shi,H., Strogantsev,R., Takahashi,N., Kazachenka,A., Lorincz,M.C., Hemberger,M. and Ferguson-Smith,A.C. (2019) ZFP57 regulation of transposable elements and gene expression within and beyond imprinted domains. *Epigenet.Chromatin*, **12**, 49.

38. Ferrón,S.R., Charalambous,M., Radford,E., McEwen,K., Wildner,H., Hind,E., Morante-Redolat,J.M., Laborda,J., Guillemot,F., Bauer,S.R. *et al.* (2011) Postnatal loss of Dlk1 imprinting in stem cells and niche astrocytes regulates neurogenesis. *Nature*, **475**, 381–387.

39. Beygo,J., Küchler,A., Gillessen-Kaesbach,G., Albrecht,B., Eckle,J., Eggermann,T., Gellhaus,A., Kanber,D., Kordaß,U., Lüdecke,H.J. *et al.* (2017) New insights into the imprinted MEG8-DMR in 14q32 and clinical and molecular description of novel patients with Temple syndrome. *Eur. J. Hum. Genet.*, **25**, 935–945.

40. Zhao,J., Ohsumi,T.K., Kung,J.T., Ogawa,Y., Grau,D.J., Sarma,K., Song,J.J., Kingston,R.E., Borowsky,M. and Lee,J.T. (2010) Genome-wide identification of polycomb-associated RNAs by RIP-seq. *Mol. Cell*, **40**, 939–953.

41. Court,F., Tayama,C., Romanelli,V., Martin-Trujillo,A., Iglesias-Platas,I., Okamura,K., Sugahara,N., Simón,C., Moore,H., Harness,J.V. *et al.* (2014) Genome-wide parent-of-origin DNA methylation analysis reveals the intricacies of human imprinting and suggests a germline methylation-independent mechanism of establishment. *Genome Res.*, **24**, 554–569.

42. Ito,M., Sferruzzi-Perri,A.N., Edwards,C.A., Adalsteinsson,B.T., Allen,S.E., Loo,T.H., Kitazawa,M., Kaneko-Ishino,T., Ishino,F., Stewart,C.L. *et al.* (2015) A trans-homologue interaction between reciprocally imprinted miR-127 and Rtl1 regulates placenta development. *Development*, **142**, 2425–2430.

43. Kitazawa,M., Hayashi,S., Imamura,M., Takeda,S., Oishi,Y., Kaneko-Ishino,T. and Ishino,F. (2020) Deficiency and overexpression of Rtl1 in the mouse cause distinct muscle abnormalities related to Temple and Kagami-Ogata syndromes. *Development*, **147**, dev185918.

44. Kitazawa,M., Sutani,A., Kaneko-Ishino,T. and Ishino,F. (2021) The role of eutherian-specific RTL1 in the nervous system and its implications for the Kagami-Ogata and Temple syndromes. *Genes Cells*, **26**, 165–179.

45. Acurzio,B., Verma,A., Polito,A., Giaccari,C., Cecere,F., Fioriniello,S., Della Ragione,F., Fico,A., Cerrato,F., Angelini,C. *et al.* (2021) Zfp57 inactivation illustrates the role of ICR methylation in imprinted gene expression during neural differentiation of mouse ESCs. *Sci. Rep.*, **11**, 13802.

46. Hara,S., Terao,M., Tsuji-Hosokawa,A., Ogawa,Y. and Takada,S. (2021) Humanization of a tandem repeat in IG-DMR causes stochastic restoration of paternal imprinting at mouse Dlk1-Dio3 domain. *Hum. Mol. Genet.*, **30**, 564–574.

47. Liu,Y., Toh,H., Sasaki,H., Zhang,X. and Cheng,X. (2012) An atomic model of Zfp57 recognition of CpG methylation within a specific DNA sequence. *Genes Dev.*, **26**, 2374–2379.

48. Ivanov,A.V., Peng,H., Yurchenko,V., Yap,K.L., Negorev,D.G., Schultz,D.C., Psulkowski,E., Fredericks,W.J., White,D.E., Maul,G.G. *et al.* (2007) PHD domain-mediated E3 ligase activity directs intramolecular sumoylation of an adjacent bromodomain required for gene silencing. *Mol. Cell*, **28**, 823–837.

49. Peng,J. and Wysocka,J. (2008) It takes a PHD to SUMO. *Trends Biochem. Sci.*, **33**, 191–194.

50. Wang,Y., Zhang,H., Chen,Y., Sun,Y., Yang,F., Yu,W., Liang,J., Sun,L., Yang,X., Shi,L. *et al.* (2009) LSD1 is a subunit of the NuRD complex and targets the metastasis programs in breast cancer. *Cell*, **138**, 660–672.

51. Zuo,X., Sheng,J., Lau,H.T., McDonald,C.M., Andrade,M., Cullen,D.E., Bell,F.T., Iacovino,M., Kyba,M., Xu,G. *et al.* (2012) Zinc finger protein ZFP57 requires its co-factor to recruit DNA methyltransferases and maintains DNA methylation imprint in embryonic stem cells via its transcriptional repression domain. *J. Biol. Chem.*, **287**, 2107–2118.

52. Ye,B., Yang,G., Li,Y., Zhang,C., Wang,Q. and Yu,G. (2020) ZNF143 in chromatin looping and gene regulation. *Front. Genet.*, **11**, 338.

53. Sapozhnikov,D.M. and Szyf,M. (2021) Unraveling the functional role of DNA demethylation at specific promoters by targeted steric blockage of DNA methyltransferase with CRISPR/dCas9. *Nat. Commun.*, **12**, 5711.

54. Lee,J., Matsuzawa,A., Shiura,H., Sutani,A. and Ishino,F. (2018) Preferable in vitro condition for maintaining faithful DNA methylation imprinting in mouse embryonic stem cells. *Genes to Cells*, **23**, 146–160.

55. Stelzer,Y., Wu,H., Song,Y., Shivalila,C.S., Markoulaki,S. and Jaenisch,R. (2016) Parent-of-Origin DNA methylation dynamics during mouse development. *Cell Rep.*, **16**, 3167–3180.

56. Swanzey,E., McNamara,T.F., Apostolou,E., Tahiliani,M. and Stadtfeld,M. (2020) A susceptibility locus on chromosome 13 profoundly impacts the stability of genomic imprinting in mouse pluripotent stem cells. *Cell Rep.*, **30**, 3597–3604.

57. Oki,S., Ohta,T., Shioi,G., Hatanaka,H., Ogasawara,O., Okuda,Y., Kawaji,H., Nakaki,R., Sese,J. and Meno,C. (2018) ChIP-Atlas: a data-mining suite powered by full integration of public ChIP-seq data. *EMBO Rep.*, **19**, e462455.